

Article

A Foldable Metal–Organic Framework with cds Topology Assembled via Four-Connected Square-Planar Single Ni²⁺-Ion Nodes and Linear Bidentate Linkers

Zhi-Chun Shi ¹, Xiaoliang Wang ², Vadym Drozd ³ and Raphael G. Raptis ^{1,*}

¹ Department of Chemistry and Biochemistry, Florida International University, Miami, FL 33199, USA; zshi008@fiu.edu

² Department of Chemistry, Northwestern University, Evanston, IL 60208, USA; xiaoliang.wang@northwestern.edu

³ Center for Study of Matter at Extreme Conditions, Florida International University, Miami, FL 33199, USA; drozdv@fiu.edu

* Correspondence: rraptis@fiu.edu

Abstract: A binary, three-dimensional (3D), foldable, Metal–Organic Framework (MOF) of formula $[\text{trans-Ni}(\text{H}_2\text{O})_2(\mu\text{-}4,4'\text{-bpy})_2](\text{ClO}_4)_2$ (**1**), with CdSO_4 (6⁵ 8), cds, topology, based on four-connected (4-c) square-planar single Ni²⁺ ion nodes and two-connected (2-c) linear rigid 4,4'-bipyridine (4,4'-bpy) ligands, was synthesized and structurally characterized via single crystal X-ray crystallography. The 41° dihedral angle between two distinct coordination environments within the 3D network of **1** produced the self-dual topology of Ni²⁺ nodes. Two rectangular 1D channels ran parallel to the crystallographic *a*-axis and *b*-axis, respectively, creating a 44.2% volume porosity, probed by gas (N₂, CO₂, and H₂) sorption studies. The PXRD, FT-IR, Raman, EDS, and SEM methods were employed for the study of **1**. A thermogravimetric analysis (TGA) showed that coordinated water molecules were readily removed upon heating, whereas the 3D lattice remained intact up to 370 °C.

Keywords: 3D MOF; cds; four-nodal; single metal atom node; bipyridine linker; foldable network



Citation: Shi, Z.-C.; Wang, X.; Drozd, V.; Raptis, R.G. A Foldable Metal–Organic Framework with cds Topology Assembled via Four-Connected Square-Planar Single Ni²⁺-Ion Nodes and Linear Bidentate Linkers. *Crystals* **2024**, *14*, 40. <https://doi.org/10.3390/cryst14010040>

Academic Editor: Kil Sik Min

Received: 4 December 2023

Revised: 24 December 2023

Accepted: 26 December 2023

Published: 28 December 2023



Copyright: © 2023 by the authors. Licensee MDPI, Basel, Switzerland. This article is an open access article distributed under the terms and conditions of the Creative Commons Attribution (CC BY) license (<https://creativecommons.org/licenses/by/4.0/>).

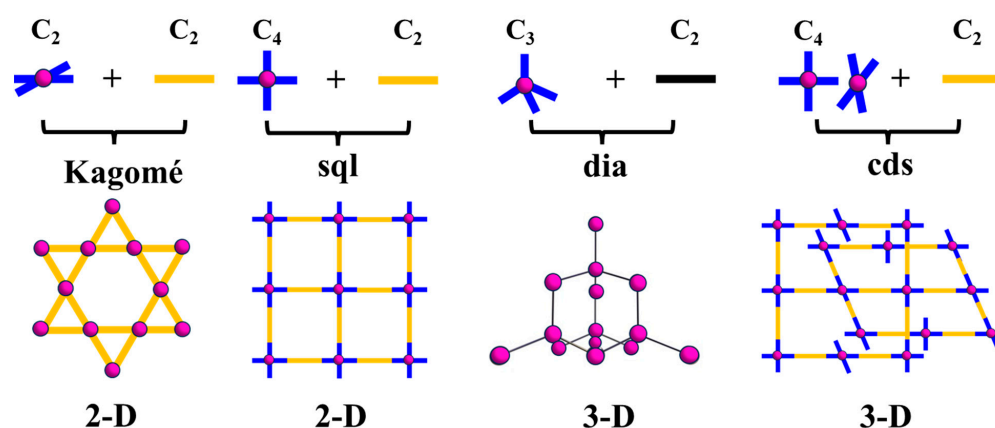
1. Introduction

Metal–Organic Frameworks (MOFs), also called porous coordination polymers (PCPs), have been extensively explored in the past three decades because of their various topological possibilities and potential applications, including chemical storage, chemical separation, sensing, catalysis, luminescence, and magnetism, etc. [1–3].

In the early days of MOF chemistry development, the discovery of new coordination polymers mainly relied on single metal ion nodes and ditopic N-donor ligands (e.g., diamines and bipyridines) because of their structural rigidity and ready accessibility [4]. At present, elaborately designed organic ligands and secondary building units (SBUs) are used in order to prepare complex structures possessing specific functions, despite the often high costs of starting materials [5]. However, because large-scale applications of MOFs will only be possible if they are economically feasible, interest in synthetic procedures using inexpensive, easily accessible starting materials (ligands and metal salts) is sustained [5]. A second desirable property of MOFs is their robustness to external conditions, such as temperature and pressure [2,3].

A literature survey shows that a few dozen polymeric structures based on N-donor ligands and single transition metal ion nodes have been documented, exemplifying a few of the many possible topologies [6]. For instance (Scheme 1), the 2D **sql** (square lattice) and **kagm** [7] (Kagomé: a lattice constructed of equilateral triangles, forming large hexagonal voids) binary networks are well documented when only single, homoleptic,

square planar transition metal centers (Fe^{2+} , Co^{2+} , Ni^{2+} , Cu^{2+} , Zn^{2+} , and Cd^{2+}) and 4,4'-bipyridyl (4,4'-bpy) ligands are used in the synthesis [8–12]. In contrast, 3D **dia** (diamond) or **pcu** (primitive cubic) networks are formed with single metal tetrahedral (4-c) nodes, e.g., $-\{[\text{Cu}(\mu\text{-}4,4'\text{-bpy})_{1.5}]\text{NO}_3 \cdot 1.25\text{H}_2\text{O}\}_n$ [13], or octahedral (6-c) nodes supported by mixed ligands, e.g., $[\text{Zn}(\mu\text{-}4,4'\text{-bpy})_2(\mu\text{-SiF}_6)] \cdot x\text{DMF}_n$ [14], respectively. Most of the time, 3D networks are formed through the aggregation of 2D lattices via supramolecular interactions ($\pi \cdot \pi$ stacking and H-bonding, etc.). Meanwhile, more than twenty 3D CdSO_4 ($6^5 8$, **cds**) networks incorporating mixed ligands have been reported in the past twenty years (for example, references [15–22] and Chart S1; Web of Science accessed November 2023). Surprisingly, an analogous **cds** network constructed with 4,4'-bpy ligands and square planar 4-c single metal nodes had been hitherto missing.



Scheme 1. Networks with four-connected single atom nodes and linear rigid linkers. The symmetry operations listed here correspond to the principal axis of the respective node or linker.

Herein, we report such a robust, porous, 3D MOF structure of **cds** topology, constructed with planar, four-connected Ni^{2+} nodes and linear ditopic 4,4'-bipyridine (4,4'-bpy) linkers. Recently, F. M. Amombo Noa et al. introduced the concept of “foldable networks” [23], and recognized **cds** as one of eight MOF topologies that can possess this property, which allows the network to “breathe” upon the sorption/desorption of guest species.

2. Materials and Methods

2.1. Materials

Solvents, ligand, and nickel salt were purchased from commercial sources: $\text{Ni}(\text{ClO}_4)_2 \cdot 6\text{H}_2\text{O}$ (99.5%) and Et_2O ($\geq 99\%$) from Thermo Scientific (Waltham, MA, USA); 4,4'-bipyridine (98%) and MeOH ($\geq 99\%$) from Sigma-Aldrich (St. Louis, MO, USA). Solvents were used without further purification. Elemental analyses (C, H, N) were performed by Galbraith Laboratories, Inc., Knoxville, TN, USA.

2.2. Physical Methods

FT-IR spectra were recorded on an Agilent 5600 FT-IR Spectrophotometer (ATR mode) in the $4000\text{--}200\text{ cm}^{-1}$ region. Raman spectra were recorded with a JASCO NRS-4100 Laser Raman Spectrometer (JASCO, Oklahoma City, OK, USA) with a green or red laser in the $4000\text{--}150\text{ cm}^{-1}$ region. Gas sorption isotherms were obtained using a Micromeritics 3Flex adsorption instrument (Micromeritics, Norcross, GA, USA). Energy dispersive spectra (EDS) and scanning electron microscopy (SEM) tests were performed on a JEOL JSM 5900LV high and low vacuum SEM (JEOL, Tokyo, Japan). The TGA was recorded with a 2950 TG Analyzer with a N_2 stream flow at the ramp of $5\text{ }^\circ\text{C}/\text{min}$. Powder X-ray diffraction (PXRD) patterns were recorded on a Rigaku BD700535-01 (Rigaku, Tokyo, Japan), $\text{Cu-K}\alpha$ radiation, $\lambda = 1.541874\text{ \AA}$.

Single-crystal X-ray diffraction (SCXRD) data were collected on a Bruker D8 QUEST CMOS (Bruker, Madison, WI, USA) system equipped with a TRIUMPH curved-crystal

monochromator and Mo-K α radiation ($\lambda = 0.71073 \text{ \AA}$) from a fine-focus X-ray tube at ambient and low temperatures using the APEX3 suite. Frames were integrated with the Bruker SAINT software (APEX3, Bruker, Madison WI, USA) package using a narrow-frame algorithm. Absorption effects were corrected using the multi-scan method (SADABS) [24]. Structures were solved with intrinsic phasing methods with ShelXT [25] and refined with ShelXL using full-matrix least-squares minimization using Olex2 [26]. All non-hydrogen atoms were refined anisotropically. Hydrogen atoms' positions were calculated and fixed via HFIX, with their thermal ellipsoids riding on those of their carbon atoms. Because refinement of the diffraction data collected at ambient temperature could not locate the disordered ClO_4^- anions, a low-temperature data set was collected for structure determination. During refinement using the low-temperature diffraction data set, ClO_4^- counterions were located; however, even at 172 K, interstitial solvents, like MeOH and H_2O , could not be refined. Thus, the Mask command [26] (equivalent to SQUEEZE in Platon) embedded in Olex2 was applied at the last stages of the structure refinement. The Crystal Maker and Olex2 software (1.5-alpha, OlexSys Ltd., Durham, UK) packages were used to simplify the network and draw the molecular diagram. ToposPro was used to conduct the topological analysis [27]. CCDC 2310766 contains the supplementary crystallographic data and can be obtained free of charge from the Cambridge Crystallographic Data Center via www.ccdc.cam.ac.uk/data_request/cif.

2.3. Synthesis

Complex 1: To a light green solution of $\text{Ni}(\text{ClO}_4)_2 \cdot 6\text{H}_2\text{O}$ (0.5 mmol, 182.85 mg) in 15 mL of MeOH, 4,4'-bipyridine (4,4'-bpy, 1.0 mmol, 156.19 mg) was added, resulting in a blueish cloudy mixture, which was stirred overnight and filtered. The blue filtrate was collected and set for crystallization through layering with Et_2O for one week, followed by the slow evaporation of the solvent mixture, which yielded blue, block-shaped crystallographic-quality crystals (Figure S1) after ten days; yield 30%. An elemental analysis for an air-dried sample; calculated (for $1 \cdot 0.14\text{MeOH} \cdot 0.40\text{H}_2\text{O}$); C, 39.90; H, 2.68; N, 9.31; found: C, 39.40; H, 2.86; N, 9.12. FT-IR (cm^{-1}): 3472 (br), 3150 (br), 1647 (m), 1610 (s), 1537 (s), 1492 (m), 1477 (m), 1417 (s), 1324 (w), 1223 (s), 1064 (s), 928 (s), 814 (s), 734 (m), 621 (s), 516 (m), 496 (m), 476 (w), 439 (w), 423 (w), 411 (w), 375 (w), and 310 (w). Raman (cm^{-1}): 1596 (s), 1494 (m), 1429 (w), 1397 (w), 1278 (s), 1208 (m), 1054 (m), 1003 (s), 906 (s), 845 (w), 759 (m), 639 (m), 606 (m), 558 (w), 438 (m), 375 (m), 295 (m), and 180 (m). Caution! Perchlorate salts can become explosive and should be used with care on a small scale.

3. Results and Discussion

3.1. Structure Description

Compound **1**, with the formula of $\{[\text{trans-Ni}(\text{H}_2\text{O})_2(\mu\text{-}4,4'\text{-bpy})_2](\text{ClO}_4)_2\}_n$, was crystallized in the orthorhombic $Ccc2$ polar space group with one half of the polymer repeat unit per asymmetric unit and the other half-unit generated by a two-fold rotation. The crystallographic data are summarized in Table 1.

Table 1. Crystallographic data for **1**.

	$\{[\text{trans-Ni}(\text{H}_2\text{O})_2(\mu\text{-}4,4'\text{-bpy})_2](\text{ClO}_4)_2\}_n$
Empirical formula	$\text{C}_{20}\text{H}_{16}\text{Cl}_2\text{N}_4\text{NiO}_{10}$
FW	606.01
Temp (K)	172
Wavelength (\AA)	0.71073
Crystal system	Orthorhombic
Space group	$Ccc2$ (No. 37)
a (\AA)	7.9447 (5)
b (\AA)	21.236 (1)
c (\AA)	22.519 (2)
V (\AA^3)	3799.3 (4)

Table 1. Cont.

$\{[trans-Ni(H_2O)_2(\mu-4,4'-bpy)_2](ClO_4)_2\}_n$	
Z	4
D(calcd) (g/cm ⁻³)	1.059
abs coeff (mm ⁻¹)	0.692
Total/indnt reflcns	25,030/3255
Refl I > 2σ(I)/param	2240/103
R _{int}	0.0702
R ₁	0.0841
wR ₂	0.2198
R ₁ (all data)	0.1222
wR ₂ (all data)	0.2673
F(000)	1240.0
GoF	1.051
CCDC No.	2310766

Figure 1a shows each Ni²⁺ center adopting an octahedral six-coordinate mode and serving as a 4-c coordinated SBU, with two H₂O at *trans* (axial) positions and four 4,4'-bpy 2-c linearly bridging ligands occupying the equatorial sites. Such combinations are typically expected to result in a **sql** network. Here, however, because of the 41° dihedral angle between the coordination planes of the consecutive Ni-centers of **1**—the term self-dual has been coined for such arrangements [15,16]—its lattice adopts the **cds** topology (Figure 1b,c). The free rotation about the Ni-N σ-bonds of **1** is the crucial feature enabling the folding of the lattice (see Section 3.3, below). The cationic framework contains ClO₄⁻ counter anions H-bonded to coordinated H₂O molecules; O⋯OClO₃, 2.854 (5) Å. A comparison of selected bond lengths and angles of **1** with those of previously reported diamagnetic mononuclear [trans-Ni(H₂O)₂(py)₄](ClO₄)₂ (Table 2) shows the corresponding metric parameters to be equal within experimental error, suggesting that **1** is also diamagnetic. Table S1 lists the bond lengths and angles for **1**.

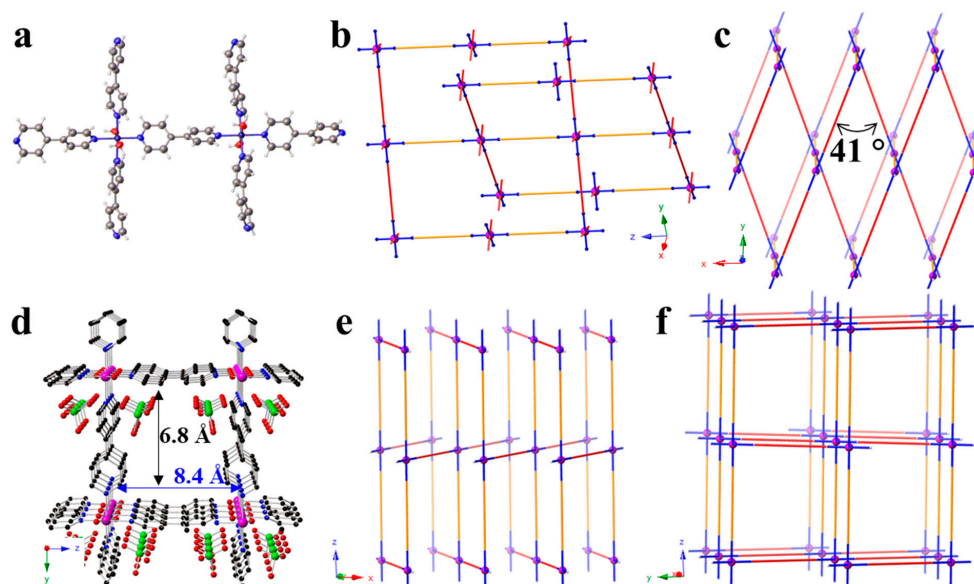


Figure 1. (a) Two types of orientations of the four-connected Ni²⁺ extended by 4,4'-bpy linkers; (b) two types of lattices formed; (c) the dihedral angle of two different lattices is 41°; (d) 1D rectangular-shaped channel with 6.8 × 8.4 Å; (e) simplified network diagram from *b*-axis; and (f) **cds** topology of the 3D framework. Color code: Ni, violet; Cl, green; O, red; N, blue; C, black.

Table 2. Selected bond lengths and angles for **1** and *[trans-Ni(H₂O)₂(py)₄](ClO₄)₂* [28].

Compound	Ni-O Å	Ni-N Å	N-Ni-N	O-Ni-N	O-Ni-O
1	2.097 (7)	2.101 (17)–2.133 (4)	177.592 (3), 180	89.165 (4)–90.8 (2)	179.397 (4)
<i>[Ni(H₂O)₂(py)₄](ClO₄)₂</i>	2.093 (6), 2.090 (6)	2.096 (7)–2.115 (7)	176.6 (3), 176.7 (3)	87.7 (3)–93.3 (3)	178.6 (3)

3.2. Topological Analysis

The simplified structure depiction of **1** (Figure 1e,f) reveals 1D rectangular channels along the crystallographic *a*-axis with approximate 6.8×8.4 Å dimensions (Figures 1d and 2a), whose aromatic walls are defined by pyridine rings (Figure 2). The pore solvent accessible voids represent 41.5% of the MOF volume (calculated with the Mercury software—2022, 3.0). Another rectangular-shaped 1D channel along the *b*-axis, with approximate 9.0×3.0 Å dimensions, is shown in Figure 2b. The total solvent accessible void volume of **1** is 1570.62 Å³, or 41.3% of the unit cell volume (calculated by PLATON, 2023.1) [29]. The ClO₄[−] anions are located at the corner of the square 1D channel running parallel to the *a*-axis (Figure 1d).

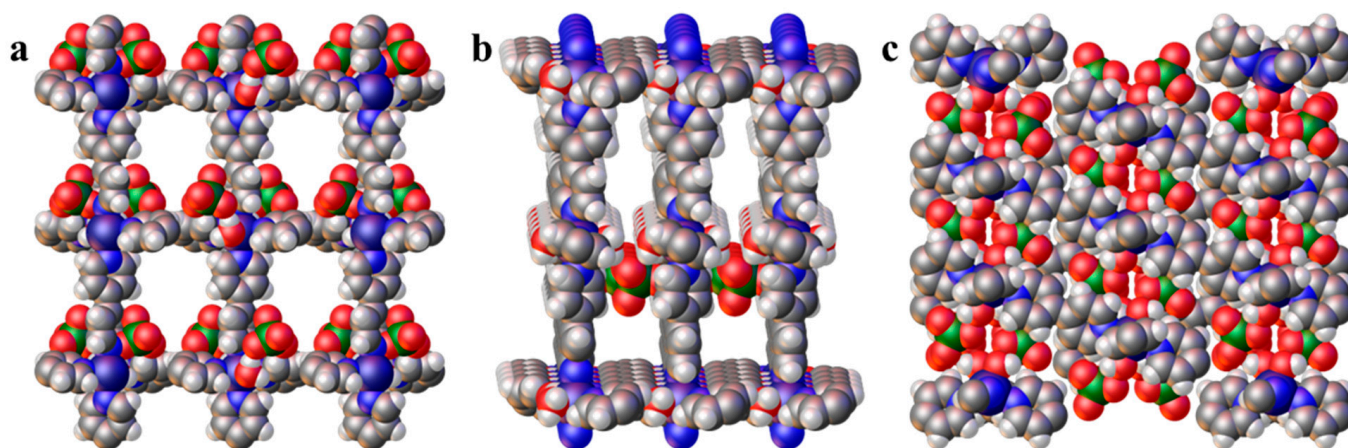


Figure 2. The diagram of the voids viewed along the *a*-axis (a) and two different angles (b,c). Color code: Ni, dark blue; Cl, green; O, red, N, blue; C, grey; H, white.

3.3. Packing Diagrams and Folding

Ignoring the coordinated H₂O molecules, which do not contribute to 3D connectivity, **1** is described as a construct of square planar Ni-nodes connected with bpy rods. In this topology, the rotation of the NiO₂N₂ coordination plane about the perpendicular N-Ni-N axis parallel to the crystallographic *c*-direction (i.e., the folding axis) allows the *bc*-planes to glide parallel to the *b*-axis, collapsing/expanding the lattice parallel to the *a*-axis (Videos S1 and S2). The folding is achievable via rotation around the *trans*-Ni-N single bonds that run parallel to the *c*-axis. We are aware of one more reported example by Choe et al. of an origamic material displaying folding motions: an MOF assembled with Zn nodes and flexible porphyrin linkers as pivoting points [30].

An FT-IR spectrum of **1** (Figure 3) shows some characteristic peaks of perchlorate, ClO₄[−], including strong and broad peaks at 1064 cm^{−1} and 621 cm^{−1} attributed to the two triply degenerate vibrations, the nondegenerate stretching vibration at 928 cm^{−1}, and the doubly degenerate vibration at 476 cm^{−1}, which point to the presence of ClO₄[−] [28,31]. In addition, the peaks at 906 cm^{−1} and 639 cm^{−1} in the Raman spectrum of **1** are consistent with the ClO₄[−] vibrations (Figure 3) [28,31].

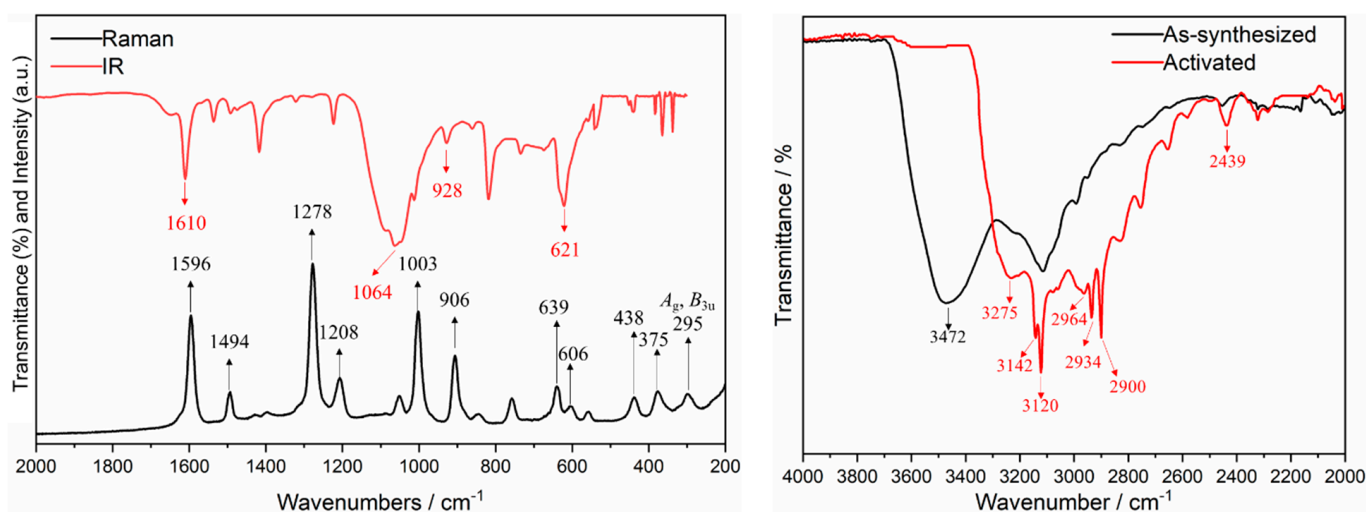


Figure 3. (Left) FT-IR and Raman; and (right) FT-IR spectrum before and after activation for **1**.

The PXRD pattern of the as-synthesized sample is in agreement with the simulated pattern, confirming the purity of the bulk crystalline samples (Figure 4a). Figure 4b shows the SEM image of compound **1** with a Au layer coated under vacuum conditions. After activation at 100 °C, the blue crystalline compound loses its interstitial and coordinated H₂O molecules (weight loss 5.3%), becoming a green-colored microcrystalline powder (Figure S3), accompanied by the disappearance of the peaks near 3500 cm⁻¹ in the FT-IR spectra (Figure 3). The removal of coordinated water molecules causes a small increase in the solvent-accessible void to 1680.92 Å³ (44.2% of unit cell volume). The presence of chlorine is evident in the EDS (three samples examined with similar results; Figure 4c and Table 3), confirming the formula proposed by the crystallography and elemental analysis (duplicate). A TGA curve (Figure 4d) establishes the thermal stability of **1** up to 370 °C, identifying it as an unusually robust material. Thermal stability up to approximately 150 °C is more typical of MOF materials assembled with single metal ion nodes and N-donor ligands.

Table 3. The EDS analysis of **1**.

Element	Mass [%]	Atom [%]
Carbon	23.5 (12)	48.6
Nitrogen	6.9 (4)	12.7
Oxygen	18.0 (9)	28.7
Chlorine	10.0 (3)	7.2
Nickel	6.3 (2)	2.8
Total	64.7	100.00

The porosity of compound **1** was assessed via gas adsorption experiments on samples activated at 150 °C under vacuum. Figure 5a suggests that there were two types of pores with average diameters of approximately 5.3 Å and 7.3 Å, respectively, in good agreement with the average dimensions of 6.0 Å and 7.6 Å, determined crystallographically (*vide supra*).

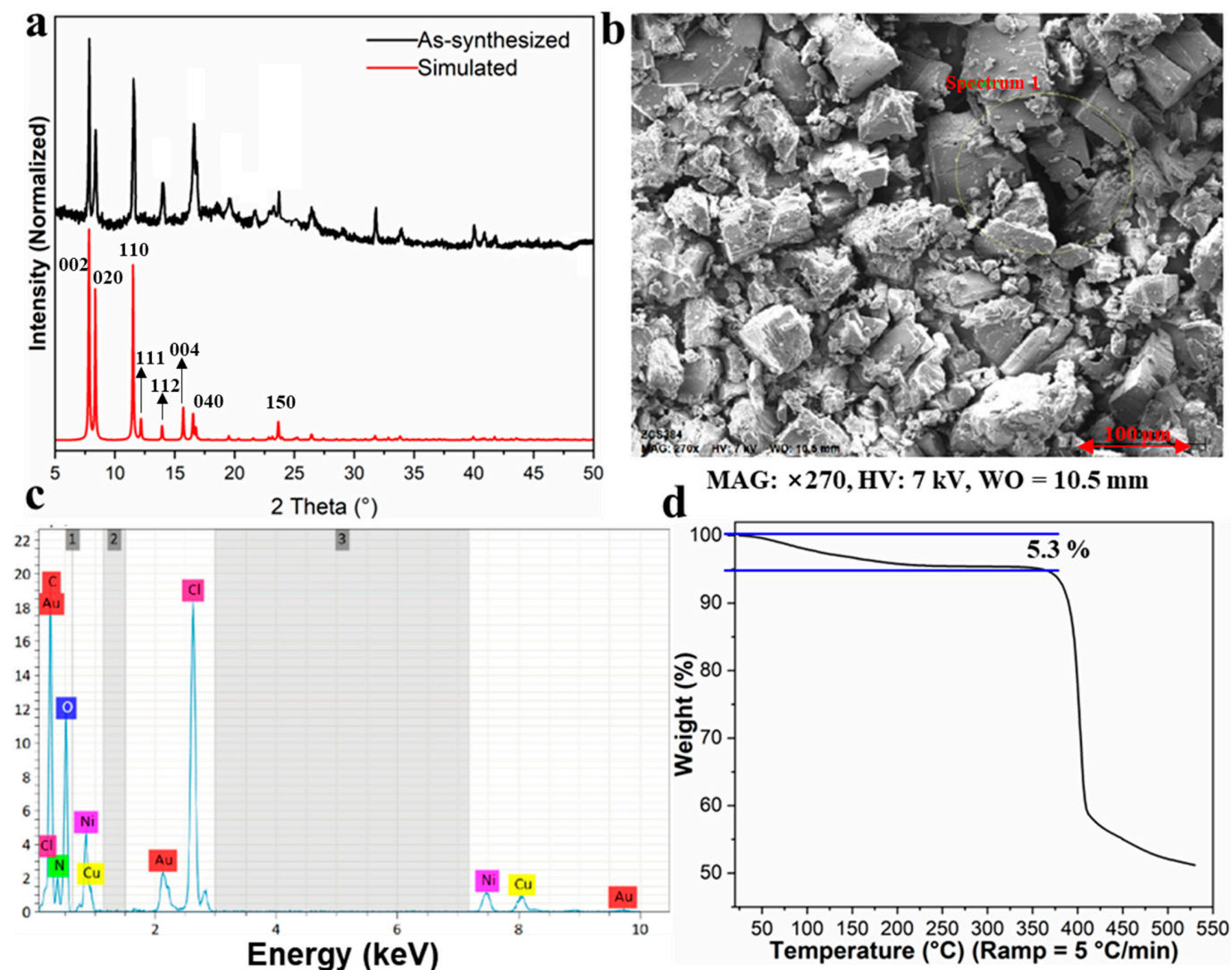


Figure 4. (a) As-synthesized and simulated PXRD pattern of **1** after activation; (b) SEM image of **1** under 7 kV at ×270 magnification; (c) EDS spectrum; and (d) TGA of **1**.

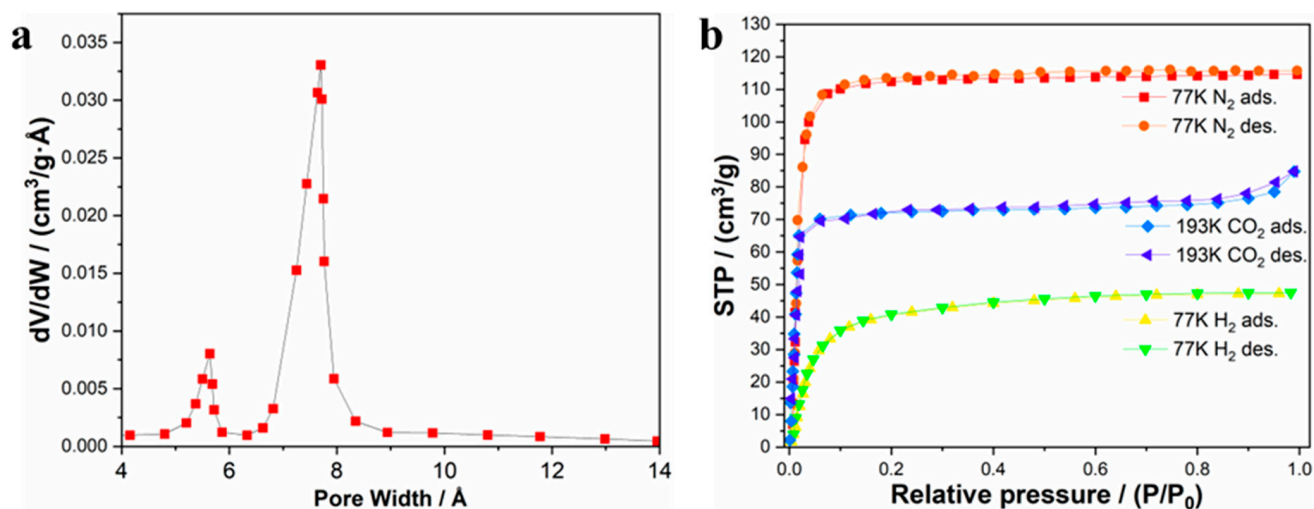


Figure 5. (a) Porous size distribution of compound **1**; and (b) gas sorption studies for **1** (red, N_2 , 77 K; green, H_2 , 77 K; and blue, CO_2 , 193 K).

N₂ adsorption data at 77 K for **1** show a typical type 1 profile, with a steep uptake increase at low pressure, leveling off at a maximum uptake capacity of 110 cm³/g. The calculated BET (Brunauer–Emmett–Teller) surface area is 450 m²/g. A similar adsorption profile is displayed by the CO₂ isothermal adsorption curve at 193 K, reaching a plateau at approximately 70 cm³/g with a further increase to 80 cm³/g in the 0.8–1.0 atm range, attributed to the guest–guest interactions [32]. At 77 K, **1** has a modest H₂ uptake capacity of approximately 41 cm³/g (Figure 5b). The N₂, H₂, and CO₂ adsorption isotherms present no evidence of breathing behavior in the 0–1 atm range, tentatively attributed to the presence of perchlorates anions in the solvent-accessible voids of the lattice, hindering network folding.

4. Conclusions

A new binary 3D MOF with **cds** topology, synthesized by a solvothermal from inexpensive starting materials. Its coordinated water molecules are readily removed via heating, while the lattice remains remarkably intact up to 370 °C. However, the most remarkable characteristic of **1** is its foldable nature, allowing the 3D structure to “breathe” without deformation of the coordination geometry of its Ni-nodes, which remain in a *D*_{4h}-symmetric local environment, without changes to bond lengths and angles. These types of foldable materials may allow for sorption/desorption studies driven by directional mechanical forces, acting like bellows. The porosity and gas sorption capacity of activated **1** are modest in comparison to the current record setting materials (7839 m²/g and 750 cm³/g) [33,34]. However, the easy removal of coordinated water molecules leaves coordinatively unsaturated Ni²⁺ sites, making **1** a good platform for further post-synthetic modification and a prospective heterogeneous catalyst [35,36]. Furthermore, the replacement of coordinated water molecules with anionic ligands (e.g., chlorides; [*trans*-NiCl₂(py)₄] is a known compound [37]) will remove the steric obstruction to folding (by perchlorate anions in **1**), allowing a wider flexibility. In any case, both **1** and its post-synthetic modified derivatives will be candidates for studies under pressure > 1 atm (the current limit of our instruments), as flexible MOFs have been attracting interest for their various anticipated exciting applications [38].

Supplementary Materials: The following supporting information can be downloaded at: <https://www.mdpi.com/article/10.3390/cryst14010040/s1>, Chart S1: Publication record for MOFs with **cds** topology; Figure S1: Photographs of the single crystal under white light from different directions; Figure S2. FT-IR and Raman spectra of compound **1**; Figure S3. Photographs of **1** before (left) and after (right) activation; Figure S4. FT-IR spectra of **1** before and after activation; Figure S5. The EDS analysis for **1** (the presence of Cu is attributed to the Cu-based tape); Table S1: Selected bond length (Å) angle (°) for **1** at 172 K; Table S2. The EDS analysis of **1**; Video S1: Video of **1** collapsing/expanding along the *a*-axis, viewed parallel to the *c*-axis. <https://youtube.com/shorts/ecfPHPMQpO8?feature=share>; Video S2. Video of 2-D planes of **1** gliding along the *b*-axis, viewed parallel to the *a*-axis. <https://youtube.com/shorts/htCFeXBuzW4?feature=share>.

Author Contributions: Z.-C.S., investigation, data analysis, writing—original draft preparation; X.W. and V.D., data collection; R.G.R., project administration, funding acquisition, supervision, writing—review and editing. All authors have read and agreed to the published version of the manuscript.

Funding: This research was funded by the National Science Foundation under Grant No. NSF-DMR-2122078. awarded to FIU.

Data Availability Statement: Data are contained within the article and supplementary materials.

Acknowledgments: The authors are grateful to Indranil Chakraborty (FIU) for his help with X-ray data refinement.

Conflicts of Interest: The authors declare no conflicts of interest.

References

1. Furukawa, H.; Cordova, K.E.; O’Keeffe, M.; Yaghi, O.M. The Chemistry and Applications of Metal-Organic Frameworks. *Science* **2013**, *341*, 1230444. [[CrossRef](#)] [[PubMed](#)]
2. Freund, R.; Zaremba, O.; Arnauts, G.; Ameloot, R.; Skorupskii, G.; Dinca, M.; Bavykina, A.; Gascon, J.; Ejsmont, A.; Goscianska, J.; et al. The current status of MOF and COF applications. *Angew. Chem. Int. Ed.* **2021**, *60*, 23975–24001. [[CrossRef](#)] [[PubMed](#)]
3. Cai, G.; Yan, P.; Zhang, L.; Zhou, H.-C.; Jiang, H.-L. Metal-Organic Framework-Based Hierarchically Porous Materials: Synthesis and Applications. *Chem. Rev.* **2021**, *121*, 12278–12326. [[CrossRef](#)] [[PubMed](#)]
4. Batten, S.R. Metal-Organic Frameworks, Design and Application. In *Topology and Interpenetration*; John Wiley & Sons, Inc.: Hoboken, NJ, USA, 2009; Chapter 3.
5. Severino, M.I.; Gkaniatsou, E.; Nouar, F.; Pinto, M.L.; Serre, C. MOFs industrialization: A complete assessment of production costs. *Faraday Discuss.* **2021**, *231*, 326–341. [[CrossRef](#)] [[PubMed](#)]
6. Cook, T.R.; Zheng, Y.-R.; Stang, P.J. Metal–Organic Frameworks and Self-Assembled Supramolecular Coordination Complexes: Comparing and Contrasting the Design, Synthesis, and Functionality of Metal–Organic Materials. *Chem. Rev.* **2013**, *113*, 734–777. [[CrossRef](#)] [[PubMed](#)]
7. Qi, M.; Zhou, Y.; Lv, Y.; Chen, W.; Su, X.; Zhang, T.; Xing, G.; Xu, G.; Terasaki, O.; Chen, L. Direct Construction of 2D Conductive Metal–Organic Frameworks from a Nonplanar Ligand: In Situ Scholl Reaction and Topological Modulation. *J. Am. Chem. Soc.* **2023**, *145*, 2739–2744. [[CrossRef](#)]
8. Adams, C.J.; Munoz, M.C.; Waddington, R.E.; Real, J.A. Cooperative Spin Transition in the Two-Dimensional Coordination Polymer [Fe(4,4′-bipyridine)₂(NCX)₂]_n·4CHCl₃ (X = S, Se). *Inorg. Chem.* **2011**, *50*, 10633–10642. [[CrossRef](#)]
9. Zhang, Y.-S.; Enright, G.D.; Breeze, S.R.; Wang, S. Coordination polymers of cobalt(II): [Co(4,4′-bpy)₂(O₂CCF₃)₂]_n and [Co(4,4′-bpy)(O₂CCH₃)₂(H₂O)₂]_n. *New J. Chem.* **1999**, *23*, 625–628. [[CrossRef](#)]
10. Yaghi, O.M.; Li, H.; Groy, T.L. A Molecular Railroad with Large Pores: Synthesis and Structure of Ni(4,4′-bpy)_{2.5}(H₂O)₂(ClO₄)₂·1.5(4,4′-bpy)·2H₂O. *Inorg. Chem.* **1997**, *36*, 4292–4293. [[CrossRef](#)]
11. Hu, F.; Yin, X.; Mi, Y.; Li, W.; Tang, X.; Ma, Z. Synthesis, structure and properties of a new copper (II) complex, [Cu₂(4,4′-bpy)₅(H₂O)₄](ClO₄)₄(4,4′-bpy)(DMF)₂(H₂O)₂. *Inorg. Chem. Commun.* **2010**, *13*, 720–723. [[CrossRef](#)]
12. Noro, S.-I.; Kitaura, R.; Kondo, M.; Kitagawa, S.; Ishii, T.; Matsuzaka, H.; Yamashita, M. Framework Engineering by Anions and Porous Functionalities of Cu(II)/4,4′-bpy Coordination Polymers. *J. Am. Chem. Soc.* **2002**, *124*, 2568–2583. [[CrossRef](#)] [[PubMed](#)]
13. Yaghi, O.M.; Li, H. Hydrothermal synthesis of a metal-organic framework containing large rectangular channels. *J. Am. Chem. Soc.* **1995**, *117*, 10401–10402. [[CrossRef](#)]
14. Subramanian, S.; Zaworotko, M.J. Porous solids by design: [Zn(4,4′-bpy)₂(SiF₆)₂]_n·xDMF, a single framework octahedral coordination polymer with large square channels. *Angew. Chem. Int. Ed. Engl.* **1995**, *34*, 2127–2129. [[CrossRef](#)]
15. Friedrichs, O.D.; O’Keeffe, M.; Yaghi, O.M. The CdSO₄, rutile, cooperite and quartz dual nets: Interpenetration and catenation. *Solid State Sci.* **2003**, *5*, 73–78. [[CrossRef](#)]
16. Friedrichs, O.D.; O’Keeffe, M. Three-periodic tilings and nets: Face-transitive tilings and edge-transitive nets revisited. *Acta Cryst. A* **2007**, *63*, 344–347. [[CrossRef](#)] [[PubMed](#)]
17. Moulton, B.; Abourahma, H.; Bradner, M.W.; Lu, J.; McManus, G.J.; Zaworotko, M.J. A new 6⁵.8 topology and a distorted 6⁵.8 CdSO₄ topology: Two new supramolecular isomers of [M₂(bdc)₂(L)₂]_n coordination polymers. *Chem. Commun.* **2003**, 1342–1343. [[CrossRef](#)] [[PubMed](#)]
18. Gao, T.; Wang, X.-Z.; Gu, H.-X.; Xu, Y.; Shen, X.; Zhu, D.-R. Two 3D metal–organic frameworks with different topologies, thermal stabilities and magnetic properties. *Cryst. Eng. Comm.* **2012**, *14*, 5905–5913. [[CrossRef](#)]
19. Liu, J.-Q.; Wu, J.; Jia, Z.-B.; Chen, H.-L.; Li, Q.-L.; Sakiyama, H.; Soares, T.; Fei, R.; Daignebonne, C.; Guillou, O.; et al. Two isorecticular metal–organic frameworks with CdSO₄-like topology: Selective gas sorption and drug delivery. *Dalton Trans.* **2014**, *43*, 17265–17273. [[CrossRef](#)]
20. Tomar, K.; Rajak, R.; Sanda, S.; Konar, S. Synthesis and Characterization of Polyhedral-Based Metal–Organic Frameworks Using a Flexible Bipyrazole Ligand: Topological Analysis and Sorption Property Studies. *Cryst. Growth Des.* **2015**, *15*, 2732–2741. [[CrossRef](#)]
21. Meng, D.-L.; Wang, X.; Tian, C.-B.; Wei, W.; Du, S.-W. Multistep Structural Transformation of a Magnetic Metal–Organic Framework: Possible Transformation Mechanism, Form Evolution, and Magnetic Properties. *Cryst. Growth Des.* **2020**, *20*, 1203–1210. [[CrossRef](#)]
22. You, Z.-X.; Wang, C.; Xiao, Y.; Guan, Q.-L.; Li, J.-X.; Xing, Y.-H.; Gao, H.-W.; Sun, L.; Bai, F.-Y. Integrated Photoresponsive Alkaline Earth Metal Coordination Networks: Synthesis, Topology, Photochromism and Photoluminescence Investigation. *Chem. Eur. J.* **2021**, *27*, 9605–9619. [[CrossRef](#)] [[PubMed](#)]
23. Amombo Noa, F.M.; Svensson Grape, E.; Brülls, S.M.; Cheung, O.; Malmberg, P.; Inge, A.K.; McKenzie, C.J.; Mårtensson, J.; Öhrström, L. Metal–Organic Frameworks with Hexakis(4-Carboxyphenyl)Benzene: Extensions to Reticular Chemistry and Introducing Foldable Nets. *J. Am. Chem. Soc.* **2020**, *142*, 9471–9481. [[CrossRef](#)]
24. Sheldrick, G.M. *SADABS. Program for Empirical Absorption Correction*; University of Gottingen: Göttingen, Germany, 1996.
25. Sheldrick, G.M. SHELXT–Integrated Space-Group and Crystal-Structure Determination. *Acta Cryst. A* **2015**, *71*, 3–8. [[CrossRef](#)] [[PubMed](#)]

26. Dolomanov, O.V.; Bourhis, L.J.; Gildea, R.J.; Howard, J.A.; Puschmann, H. OLEX2: A Complete Structure Solution, Refinement and Analysis Program. *J. Appl. Cryst.* **2009**, *42*, 339–341. [[CrossRef](#)]
27. Blatov, V.A.; Shevchenko, A.P.; Proserpio, D.M. Applied topological analysis of crystal structures with the program package ToposPro. *Cryst. Growth Des.* **2014**, *14*, 3576–3586. [[CrossRef](#)]
28. Long, G.J.; Clarke, P.J. Crystal and molecular structures of trans-tetrakis(pyridine)dichloroiron(II), -nickel(II), and -cobalt(II) and trans-tetrakis(pyridine)dichloroiron(II) monohydrate. *Inorg. Chem.* **1978**, *17*, 1394–1401. [[CrossRef](#)]
29. Spec, A.L. Structure validation in chemical crystallography. *Acta Crystallogr. Sect. D Biol. Crystallogr.* **2009**, *65*, 148–155. [[CrossRef](#)] [[PubMed](#)]
30. Jin, E.; Lee, I.S.; Yang, D.C.; Moon, D.; Nam, J.; Cho, H.; Kang, E.; Lee, J.; Noh, H.-J.; Min, S.K.; et al. Origamic Metal–Organic Framework toward Mechanical Metamaterial. *Nat. Commun.* **2023**, *14*, 7938. [[CrossRef](#)]
31. Holló, B.B.; Petruševski, V.M.; Kovács, G.B.; Franguelli, F.P.; Farkas, A.; Menyhárd, A.; Lendvay, G.; Sajó, I.E.; Nagy-Bereczki, L.; Pawar, R.P.; et al. Thermal and spectroscopic studies on a double-salt-type pyridine–silver perchlorate complex having κ^1 -O coordinated perchlorate ions. *J. Therm. Anal. Calorim.* **2019**, *138*, 1193–1205. [[CrossRef](#)]
32. Yang, S.; Sun, J.; Ramirez-Cuesta, A.J.; Callear, S.K.; David, W.I.F.; Anderson, D.; Newby, R.; Blake, A.J.; Parker, J.E.; Tang, C.C.; et al. Selectivity and direct visualization of carbon dioxide and sulfur dioxide in a decorated porous host. *Nat. Chem.* **2012**, *4*, 887–894. [[CrossRef](#)]
33. Hönicke, I.M.; Senkovska, I.; Bon, V.; Baburin, I.A.; Bönisch, N.; Raschke, S.; Evans, J.D.; Kaskel, S. Balancing Mechanical Stability and Ultrahigh Porosity in Crystalline Framework Materials. *Angew. Chem. Int. Ed.* **2018**, *57*, 13780–13783. [[CrossRef](#)] [[PubMed](#)]
34. Millward, A.R.; Yaghi, O.M. Metal–Organic Frameworks with Exceptionally High Capacity for Storage of Carbon Dioxide at Room Temperature. *J. Am. Chem. Soc.* **2005**, *127*, 17998–17999. [[CrossRef](#)] [[PubMed](#)]
35. Rosen, A.S.; Notestein, J.M.; Snurr, R.Q. Structure–Activity Relationships That Identify Metal–Organic Framework Catalysts for Methane Activation. *ACS Catal.* **2019**, *9*, 3576–3587. [[CrossRef](#)]
36. Cohen, S.M. Postsynthetic Methods for the Functionalization of Metal–Organic Frameworks. *Chem. Rev.* **2012**, *112*, 970–1000. [[CrossRef](#)]
37. Cisterna, J.; Artigas, V.; Fuentealba, M.; Hamon, P.; Manzur, C.; Dorcet, V.; Hamon, J.-R.; Carrillo, D. Nickel(II) and copper(II) complexes of new unsymmetrically-substituted tetradentate Schiff base ligands: Spectral, structural, electrochemical and computational studies. *Inorg. Chim. Acta* **2017**, *462*, 266–280. [[CrossRef](#)]
38. Schneemann, A.; Bon, V.; Schwedler, I.; Senkovska, I.; Kaskel, S.; Fischer, R.A. Flexible metal-organic frameworks. *Chem. Soc. Rev.* **2014**, *43*, 6062–6096. [[CrossRef](#)]

Disclaimer/Publisher’s Note: The statements, opinions and data contained in all publications are solely those of the individual author(s) and contributor(s) and not of MDPI and/or the editor(s). MDPI and/or the editor(s) disclaim responsibility for any injury to people or property resulting from any ideas, methods, instructions or products referred to in the content.